Available online at www.sciencedirect.com
ScienceDirect
Journal of Sound and Vibration 320 (2009) 990–1003
JOURNAL OF SOUND AND VIBRATION
www.elsevier.com/locate/jsvi

Numerical prediction of the quality of an anechoic chamber in the low frequency range

S. Schneider*

CNRS/LMA, 31 chemin Joseph-Aiguier, 13402 Marseille Cedex 20, France

Received 12 June 2007; received in revised form 28 May 2008; accepted 18 August 2008
Handling Editor: R.J. Astley
Available online 23 October 2008

Abstract

The present work focuses on the numerical prediction of the quality of an anechoic chamber in the planning stage. The quality of any numerical prediction is determined by the quality of the modeling procedure used to account for the wall treatment in the numerical simulation. Based on experimental data, this study shows that the use of a local admittance condition to account for the wall treatment is not suitable in the low-frequency range. A new type of boundary condition is described, in which the scalar admittance is replaced by a frequency-dependent admittance matrix. This matrix is calculated from the parameters of the absorbing material, the geometry of the acoustic lining and its mounting conditions. An error estimator is also presented, which makes it possible to check the accuracy of the boundary condition developed. With the boundary condition developed and applied here, the quality of an anechoic chamber was accurately predicted.

1. Introduction

Anechoic chambers are widely used to perform acoustical measurements under conditions simulating free-field sound propagation. Designing chambers of this kind is time consuming and costly, however.

Besides the acoustical properties of the lining, other properties such as the environmental impact and fire resistance are increasingly important aspects, which have given rise to the development of new materials. The quality of a lining is generally assessed based on its absorption coefficient under normal incidence of plane waves. The cut-off frequency of an anechoic chamber is defined as the lowest frequency at which the absorption coefficient α reaches a value of $\alpha = 0.99$. To avoid the time-consuming experiments required to test various possible configurations of an acoustic lining, numerical simulations are often used to determine the absorption coefficient of a sample of the lining. Most of these numerical simulations have been performed using either analytical models such as the double porosity model [1,2] or numerical methods such as the finite element method (FEM) [3–5], the boundary element method (BEM) [6] or the boundary-condition-transfer algorithm [7] to analyze the performance of an acoustic lining under normal incidence of plane waves. Little attention has been paid, however, to the fact that the lining in an anechoic chamber is subjected to loads other

*Tel.: +33 4 91 16 41 55; fax: +33 4 91 16 40 80.
E-mail address: schneider@lma.cnrs-mrs.fr

0022-460X/$ - see front matter © 2008 Elsevier Ltd. All rights reserved.
doi:10.1016/j.jsv.2008.08.019

than plane waves. In the present study, it is proposed to investigate the conditions under which the commonly used absorption coefficient can serve to predict the quality of an anechoic chamber using numerical simulations.

In numerical simulations of this kind, the acoustic lining is generally modeled in the form of a boundary condition at the air/lining interface Γ_Y. In its most general form, this boundary condition can be expressed as

$$v_{\mathbf{n}}(x) = Y(x,y)p(y) \quad \forall x,y \in \Gamma_Y. \tag{1}$$

In this form, the normal fluid velocity $v_{\mathbf{n}}$ at a single point $x \in \Gamma_Y$ is linked to the sound pressure p at all points at the air/lining interface Γ_Y via the function $Y(x,y)$, which is often referred to as the acoustic admittance. Note that the function $Y(x,y)$ can be complex valued and frequency dependent. Using the above relation enables one to replace the unknown surface velocity $v_{\mathbf{n}}$ appearing in the surface integrals of the weak formulation of the time harmonic Helmholtz equation

$$\int_{\Gamma_Y} p v_{\mathbf{n}} \,\mathrm{d}\Gamma = \int_{\Gamma_Y} p\, Yp \,\mathrm{d}\Gamma_Y \tag{2}$$

in the finite element context, or

$$\int_{\Gamma_F} \phi(x,y) v_{\mathbf{n}} \,\mathrm{d}\Gamma_Y = \int_{\Gamma_F} \phi(x,y)\, Yp(x) \,\mathrm{d}\Gamma_Y \tag{3}$$

when the boundary integral formulation is used, where $\phi(x,y)$ denotes the fundamental solution of the Helmholtz equation. Thereafter, the sound pressure p is the only unknown in the numerical solution of the corresponding equations. The quality of any numerical prediction is determined by the quality of the modeling procedure used to account for the acoustic treatment of the wall in the numerical simulation.

Two methods of modeling the acoustic lining of an anechoic chamber in a numerical analysis are compared here. The purpose of the numerical simulation is to predict the 1.5 dB region of an anechoic chamber, based either on experimental data obtained in impedance tube experiments carried out on a sample of the lining, or using an even more general approach based on the knowledge of the acoustical properties of the material with which it is proposed to make the lining, and hence to predict the quality of the future anechoic chamber in its planning stage. The study presented here focuses in particular on the low-frequency range, where designing an efficient acoustic lining is most difficult.

Experimental data obtained on the large anechoic chamber at the Laboratoire de Mécanique et d'Acoustique (LMA) in Marseille serve as reference values for assessing the quality of the various numerical models tested. The anechoic chamber at the LMA has inner dimensions of $5.4 \times 6.3 \times 11.4\,\mathrm{m}^3$, measured from wedge tip to wedge tip. Outer walls of the chamber are made of reinforced concrete. The acoustic lining consists of 3720 melamine wedges. Each wedge consists of a rectangular parallelepiped measuring $0.3 \times 0.3 \times 0.4\,\mathrm{m}^3$, forming the base of the wedge, and a tapering section of 0.7 m in length. The base of the wedges is clamped in an iron wire frame leaving a 0.25 m air gap behind the lining. The performance of the anechoic chamber at the LMA in the 20–200 Hz frequency range was determined by measuring the sound pressure radiated by a bass-reflex box placed at a distance of 1.6 m above the tips of the bottom wedges with a spatial resolution of $\Delta s = 0.2$ m. A second microphone placed 0.25 m above the plane of the suspension of the loudspeaker membrane was used as the reference microphone to check the stability of the sound source. A pure sine-tone excitation was used. The sound pressure was recorded along a traverse line running parallel to one wall (see Fig. 1). A numerical model of the bass-reflex box (see Ref. [8]) was used to determine the sound field radiated under free-field conditions. The walls of the wooden box were assumed to be motionless. This assumption was checked by measuring the displacement of the walls.

The left sub-figure in Fig. 2 compares the sound pressure recorded by the reference microphone with the sound pressure given by the numerical model. Good agreement was observed over the entire frequency range. The sound pressure recorded and that directly determined by the numerical model when the microphone was positioned on the traverse line nearest to the sound source are shown in the right sub-figure in Fig. 2. Perturbations are clearly visible in the experimental data, but the mean source strength of the sound source is correctly given by the numerical model. It can therefore be assumed that the numerical model for the YAMAHA

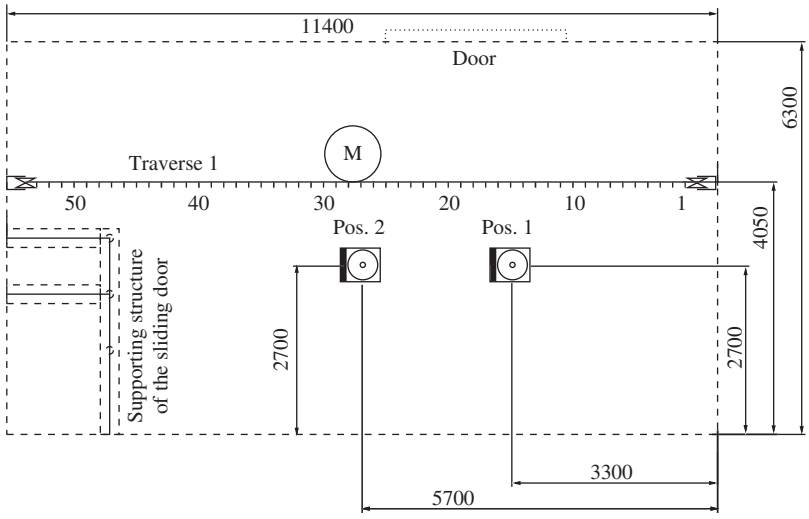

Fig. 1. Positions of the traverse lines and sound sources in the anechoic chamber. The encircled M indicates the position of the stepping motor controlling the microphone.

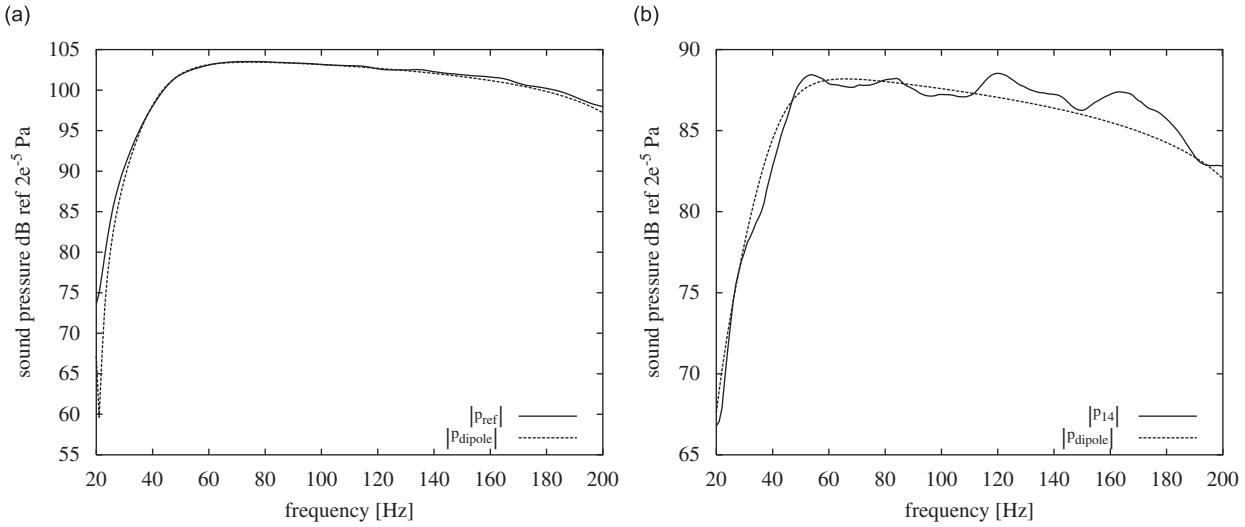

Fig. 2. Sound pressure recorded in the anechoic chamber by the reference microphone (labeled 'p_{ref}') (in sub-figure (a)) and at the microphone position on the traverse line nearest to the sound source (labeled 'p_{14}') (in sub-figure (b)) superimposed on the sound pressure created by the numerical model of the vented box (labeled 'p_{dipole}') at the corresponding positions.

SW 118IV bass-reflex box shows free-field behavior with an acceptable level of accuracy in the frequency range of interest.

From the measured sound pressure p_{exp} and the sound pressure p_{inc} generated by the sound source, the deviation from free-field conditions of the chamber was calculated from

$$L_p(x) = 20\log\left(\left|\frac{p_{\mathrm{exp}}(x)}{p_{\mathrm{inc}}(x)}\right|\right). \tag{4}$$

The maximum difference allowed between the measured and the theoretical free-field levels according to ISO 3745 and ANSI S12.35 is ± 1.5 dB at frequencies below 630 Hz. A region where the difference is smaller than the required ± 1.5 dB will be called the 1.5 dB region. The size of this region may depend on the frequency and the location of the acoustic source in the chamber.

The rest of this paper is organized as follows: Section 2 deals with the accuracy of the frequently applied local admittance model. In Section 3, a more general surface admittance model is presented. This model is obtained by localizing the non-local reaction of an absorbing material.

2. Local admittance condition

The most common geometric model used to simulate an anechoic chamber numerically is based on a rectangular cavity. In models of this kind, the real geometry of the acoustic lining (wedges made of absorbing material) is replaced by a flat surface. The latter is given an appropriate surface admittance to account for the behavior of the real acoustic lining. The advantages of models of this kind are twofold. First, this simple geometry is easy to handle using either FEM, BEM or image source modeling procedures. Second, easily available results of an impedance tube experiment are often used to obtain the surface conditions required. However, the fact that the value measured is valid only at normal incidence of plane waves is often overlooked.

Based on the experimental data available on the anechoic chamber at the LMA, the frequency domain where this model yields the most reliable results was determined. The acoustic lining of the large anechoic chamber consists of 3720 melamine wedges with a tapering section 0.7 m in length. The base of the wedges has a rectangular cross section $0.3 \times 0.3\,\mathrm{m}^2$ in size and a length of 0.4 m. The individual wedges are held in place by means of an iron wire frame screwed onto wooden bars. Three different surface admittance values were used to simulate the acoustic lining of this anechoic chamber in the following numerical simulations.

(1) The surface admittance of a 4×4 sample of the wedges constituting the acoustic lining measured in the large impedance tube at the LMA. Wedges were placed in the tube without any additional fixation.
(2) The surface admittance obtained by numerically simulating an impedance tube experiment, taking the mounting conditions of the wedges present in the anechoic chamber into account. Numerical simulation was found to be necessary here as the specific configuration (wedges held in place by an iron wire frame) could not be analyzed using the experimental facilities available at the LMA.
(3) The surface admittance calculated via

$$Y_3 = \frac{1}{\varrho c}\frac{1-\sqrt{1-\alpha_2}}{1+\sqrt{1-\alpha_2}} \tag{5}$$

from the absorption coefficient α obtained in the numerical simulation. This corresponds to the often observed situation where only the absorption coefficient of a material is communicated by manufacturers and the quality of the lining is therefore judged from the value of this coefficient.

The various local surface admittances Y_i and the corresponding absorption coefficients are shown in Fig. 3. The admittances Y_i were applied to a rectangular cavity measuring $5.4 \times 6.3 \times 11.4\,\mathrm{m}^3$, which corresponds to the inner dimensions of the anechoic chamber at the LMA. Sound propagation in the chamber was modeled using the BEM. The sound pressure in the cavity and on its surface was obtained as the solution of

$$c(y)p(y) + \int_{\Gamma_F} \frac{\partial\phi(x,y)}{\partial\mathbf{n}} p(x)\,\mathrm{d}\Gamma_F - \mathrm{i}\omega\rho Y_i \int_{\Gamma_F} \phi(x,y)p(x)\,\mathrm{d}\Gamma_F = \mathrm{i}\omega\rho \int_{\Gamma_F} \phi(x,y)v_{\mathbf{n}}^0 \tag{6}$$

The term $v_{\mathbf{n}}^0$ denotes a given normal surface velocity which is used to model the sound source. The walls of the cavity were meshed using 3720 elements resulting in a mesh size of 0.3 m. Linear discontinuous basis functions were used to discretize the sound pressure p in Eq. (6). The results of the numerical simulation are compared in Figs. 4 and 6 with the experimental data obtained with the sound source in two positions. The sub-figure (a) in Figs. 4 and 6 shows the 1.5 dB region measured in the large anechoic chamber at the LMA. Blank areas indicate regions not belonging to the 1.5 dB region. The scale bar on the left of each sub-figure gives the distance on the traverse line, where "0" is the position nearest to the sound source. Scale bar on the right of each sub-figure gives the total distance between microphone and sound source. Experimental results show that significant deviations from free-field conditions occur in the 100–160 Hz frequency range. In addition,

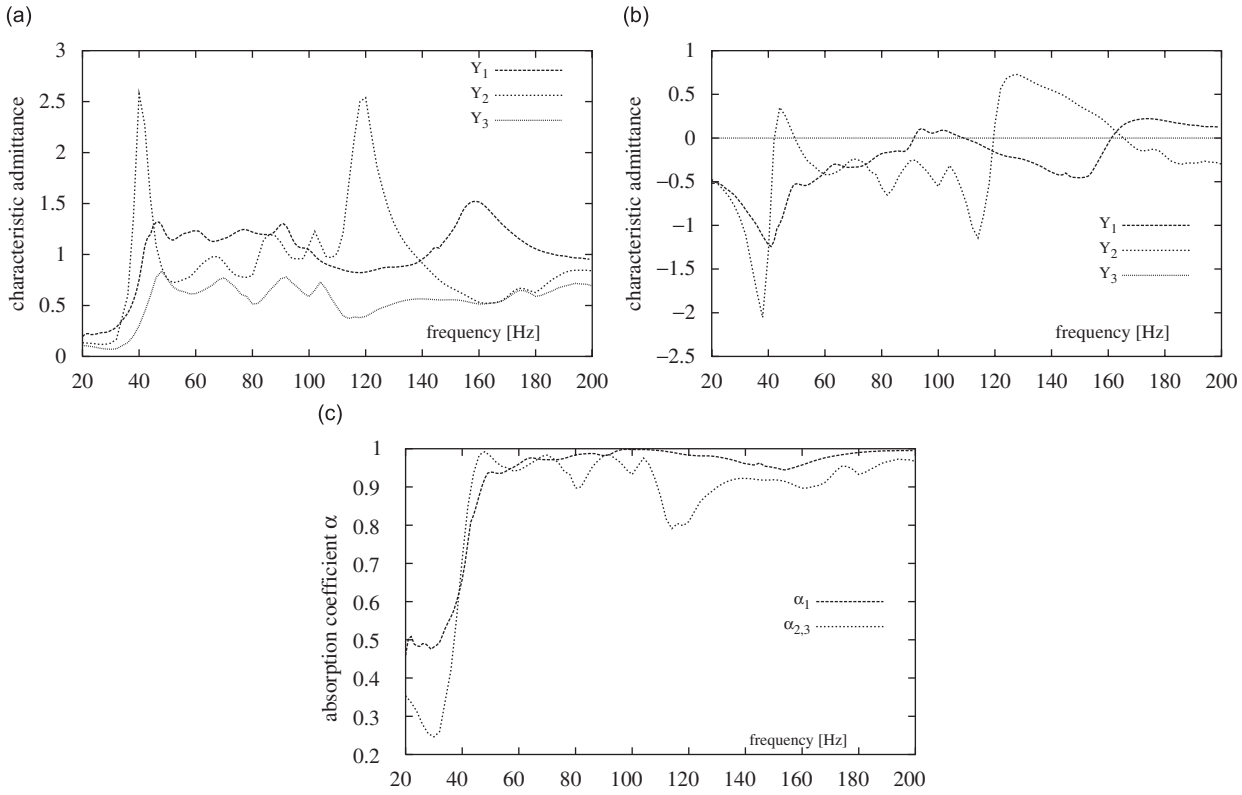

Fig. 3. Various local surface admittances and corresponding absorption coefficients used to model the acoustic lining. Sub-figure (a) real part and sub-figure (b) imaginary part of the admittance and sub-figure (c) the corresponding absorption coefficients.

the acoustical behavior of the chamber was found to be asymmetric in the 170–190 Hz frequency range. The sub-figure (b) in Figs. 4 and 6 gives the numerical results obtained using the surface admittance Y_1 based on measurements performed in the impedance tube neglecting the real mounting conditions. Results of the simulation with Y_2 and Y_3 are given in the sub-figures (c) and (d), respectively.

Assessing the quality of numerical predictions using a rigorous numerical indicator is not an easy task. First, even a slight frequency shift in the numerical results will cause an indicator of this kind to suggest the occurrence of significant errors unless averaging is performed over a wide frequency range although the numerical results may map the overall shape of the 1.5 dB region measured quite accurately. Second, the asymmetry of the chamber observed in the 170–190 Hz frequency range cannot be predicted by any of the numerical models in use, as the surface admittance is always assumed to be uniform. However, two criteria were defined for assessing the quality of the numerical predictions.

The first criterion was the number of frequency/position pairs correctly predicted to be present within the 1.5 dB region relative to all the pairs actually located within that region if there were some; otherwise, the value zero is assigned. The second criterion was the percentage of frequency/position pairs erroneously predicted to be present within the 1.5 dB region relative to the total number of actual pairs. Hence, a reliable prediction is characterized by a value of approximately one in the case of indicator C1 and approximately zero in that of indicator C2. With source position two, only microphone positions with a negative distance on the traverse line were used to calculate the indicators, to eliminated the effects of the asymmetry of the chamber. With source position one, only points at a distance on the traverse line of less than $r = 5.2$ m, which corresponds to the situation of traverse one and source position two, were used.

The values and means of both indicators obtained in the 40–200 Hz frequency range with the three surface admittances are given in Fig. 5 with the sound source placed in position two and in Fig. 7 with the sound source placed in position one (see Figs. 5 and 7).

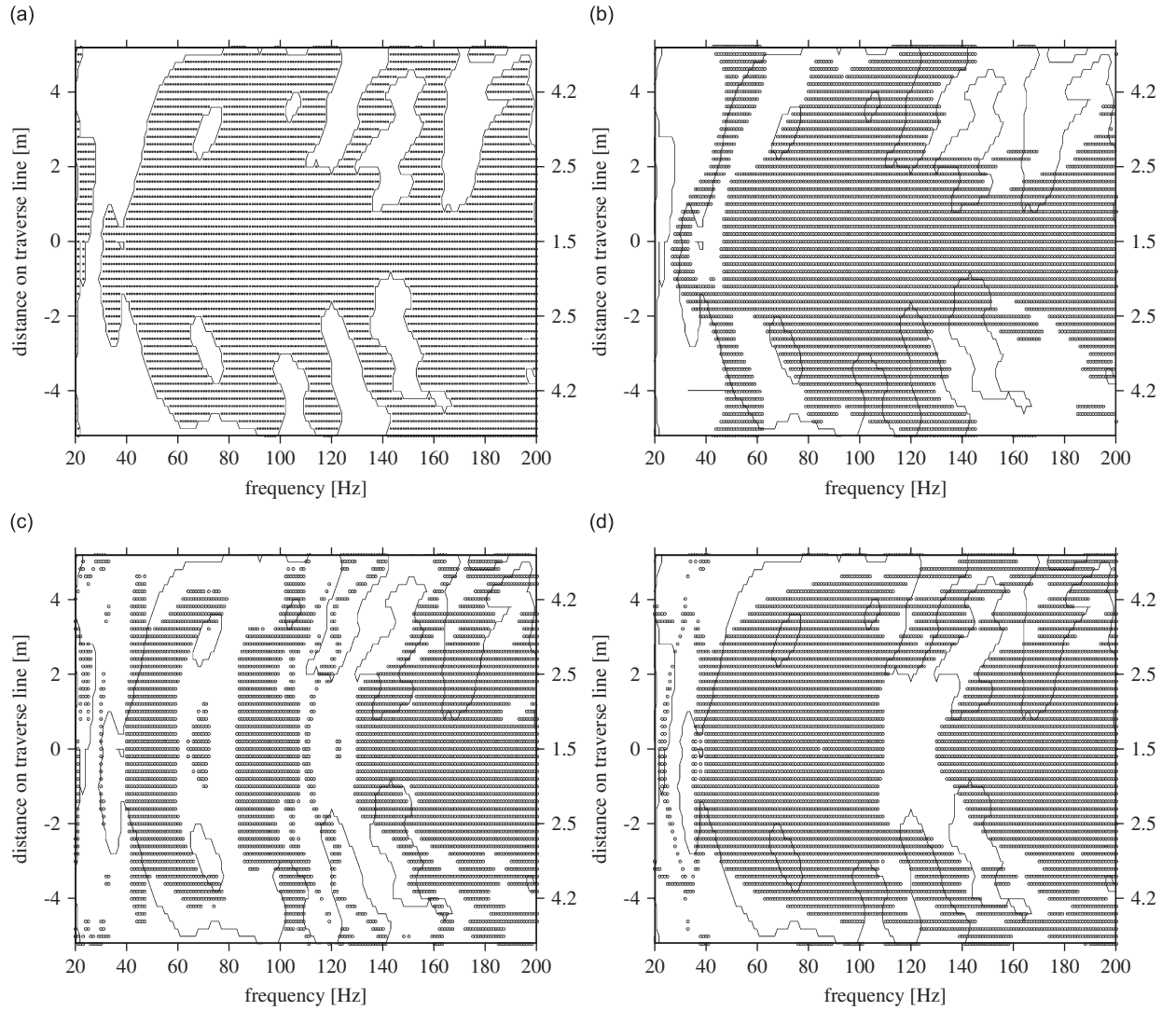

Fig. 4. 1.5 dB region measured in the large anechoic chamber at the LMA (sub-figure (a)). 1.5 dB region obtained by performing numerical simulations with various local surface admittances; sub-figure admittance (b) Y_1, sub-figure (c) admittance Y_2 and sub-figure (d) real-valued admittance Y_3. Sound source placed in the center of the chamber.

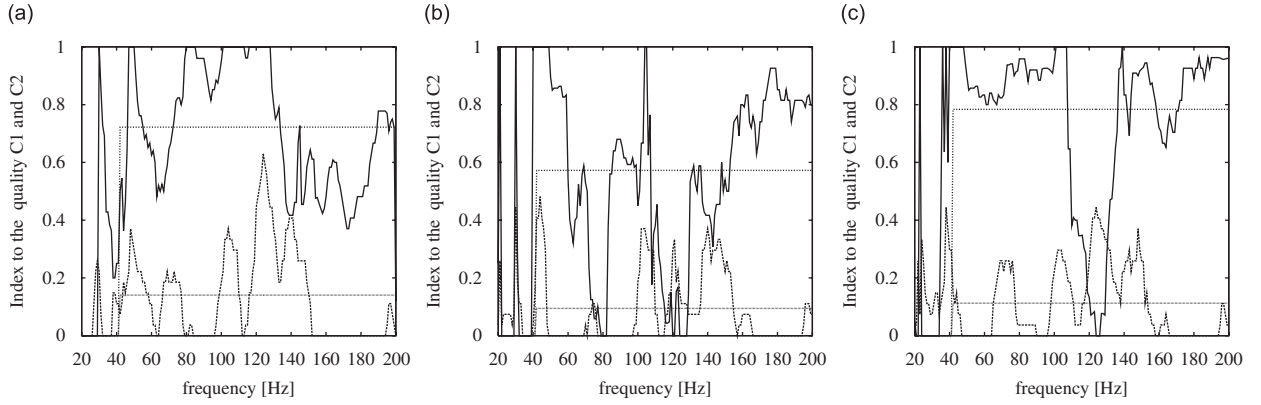

Fig. 5. Index to the quality of the predictions of the 1.5 dB region with various surface admittance values. The upper curves give indicator C1 and the mean value obtained and lower curves give indicator C2 and the mean value obtained. Sub-figure (a) admittance Y_1, sub-figure (b) admittance Y_2 and sub-figure (c) admittance Y_3. Sound source placed in the center of the chamber.

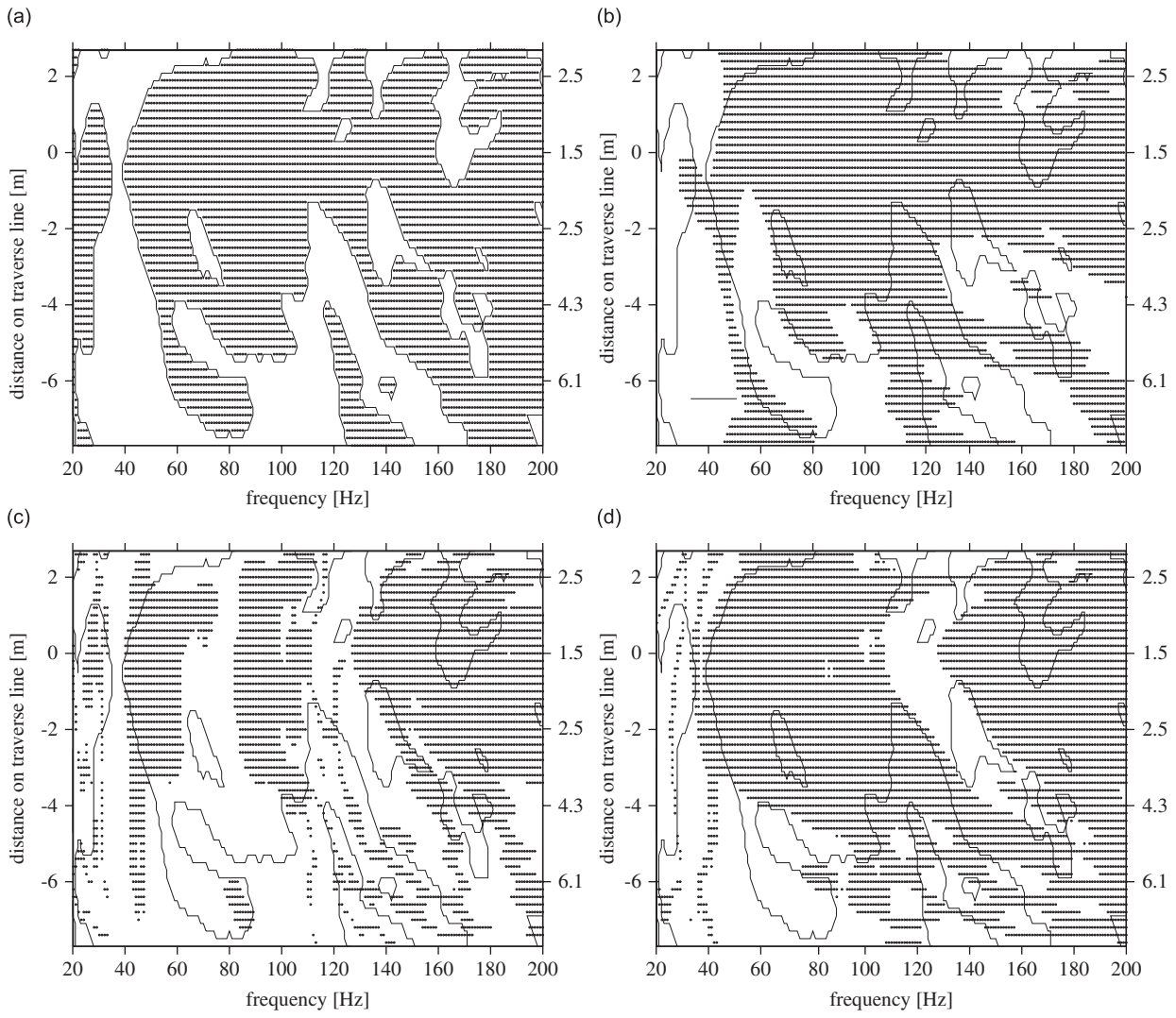

Fig. 6. 1.5 dB region measured in the large anechoic chamber at the LMA (sub-figure (a)). 1.5 dB region obtained by performing numerical simulations with various local surface admittance values; sub-figure (b) admittance Y_1, sub-figure (c) admittance Y_2 and sub-figure (d) real-valued admittance Y_3. Sound source placed at an eccentric position in the chamber.

The numerical model based on the local admittance failed to predict the quality of the chambers at frequencies below ≈ 150 Hz, regardless of the admittance applied; although the numerical indicator developed above indicates a correct prediction of the 1.5 dB region for $\approx 80\%$ of the frequency/position pairs. This is mainly due to the fact that in the 60–100 Hz frequency range, there exists quite a large 1.5 dB region. But the numerical simulations do not predict the overall shape of the 1.5 dB region measured. In particular the perturbations occurring in the 100–160 Hz frequency range were not correctly predicted by the numerical model. At higher frequencies, the surface admittances Y_2 and Y_3 can be used to assess the quality of the anechoic chamber with a reasonably good accuracy. However, surface admittance Y_3 shows a general tendency to overestimate the absorption of the lining at frequencies below 150 Hz.

Surface admittance Y_1 does not reflect the behavior of the acoustic lining in the chamber over the entire frequency range. This failure may be attributable to the fact that the mounting conditions of the lining of the anechoic chamber were not taken into account when the experiment was carried out in the impedance tube. The acoustical behavior of a material such as melamine foam is determined by the displacement of its frame,

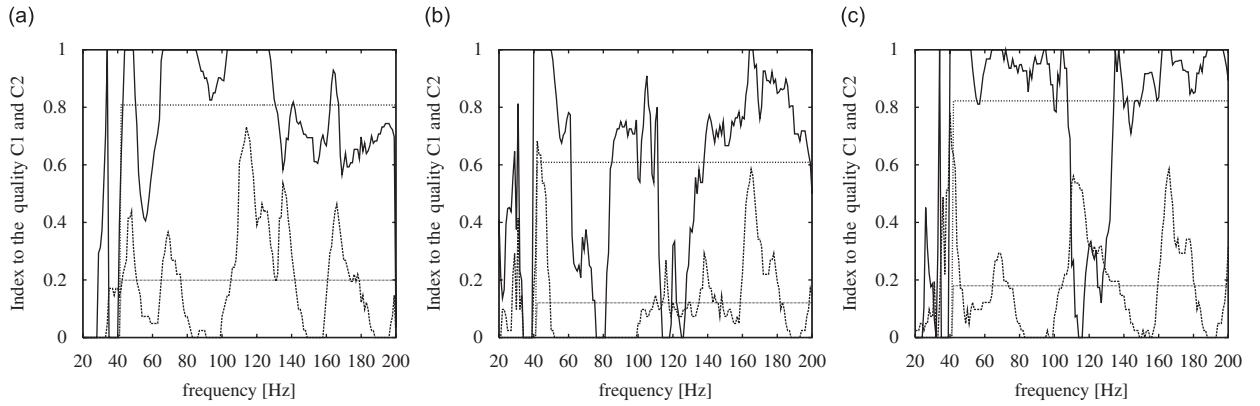

Fig. 7. Index to the quality of the predictions of the 1.5 dB region for various surface admittance values. Upper curves give indicator C1 and the mean value obtained and lower curves give indicator C2 and the mean value obtained. Sub-figure (a) admittance Y_1, sub-figure (b) admittance Y_2 and sub-figure (c) admittance Y_3. Sound source placed at an eccentric position in the chamber.

however. The mounting conditions therefore have a significant impact on the behavior of the material and must be carefully taken into account when experiments are carried out in an impedance tube.

To illustrate the difference between real and complex valued admittances (admittance Y_2 and Y_3 used above) the following situation will be studied. The admittance value corresponding to free-field conditions in the case of a monopole sound source is the admittance of a spherical wave

$$Y = \frac{1}{\varrho c}\left[\frac{\mathbf{r}\cdot\mathbf{n}}{|\mathbf{r}|} + \mathrm{i}\frac{\mathbf{r}\cdot\mathbf{n}}{|\mathbf{r}|^2}\frac{1}{k}\right] \tag{7}$$

with the vector $\mathbf{r} = \mathbf{x} - \mathbf{y}$ pointing from the sound source to a point $\mathbf{x}$ on the surface and $\mathbf{n}$ the normal vector of the surface at point $\mathbf{x}$. It becomes clear that the surface admittance value Y given by Eq. (7) depends on the position of the source and the position on the surface. To reduce the effect of this spatial dependency, the source should be placed as far as possible from the walls.

Eq. (7) further shows that the real part of the specific admittance $\tilde{Y} = \varrho c Y$ must always be smaller than or equal to one, and that the imaginary part must tend to zero when the wavenumber k tends to infinity. As most absorbing materials become increasingly absorbent with increasing frequencies, causing $\mathrm{Re}(\tilde{Y}) \leqslant 1$ and $\mathrm{Im}(\tilde{Y}) \to 0$, the absorption coefficient α, which always leads to a real-valued admittance with $\mathrm{Re}(\tilde{Y}) \leqslant 1$, can be seen to be a suitable means of characterizing an acoustic lining in the high-frequency range. But at low frequencies, where values of the surface admittance with $\mathrm{Re}(\tilde{Y}) > 1$ commonly occur with most absorbing materials, the absorption coefficient α is not suitable for characterizing an acoustic lining, as Eq. (5) always leads to $\mathrm{Re}(\tilde{Y}) \leqslant 1$. A numerical example is given here to illustrate the above findings. The 1.5 dB region of a fictitious anechoic chamber with three acoustic linings with $\tilde{Y}_1 = 0.9$, $\tilde{Y}_2 = 1$ and $\tilde{Y}_3 = 1.1$ was assessed using the above numerical model. The results obtained are given in Fig. 8. They show that although all three linings would have been judged suitable based on their absorption coefficients $\alpha_1 = 0.997$, $\alpha_2 = 1$ and $\alpha_3 = 0.997$, there are significant differences in the size of the 1.5 dB region. Hence judging the quality of an acoustic lining from its absorption coefficient alone may lead to inaccurate results if no further information about the admittance value is available.

The findings obtained in this section can be summarized as follows: replacing the real geometry of an acoustic lining by a flat surface and applying a local surface admittance yields a numerical model that can be used to predict the 1.5 dB region of the anechoic chamber at the LMA at frequencies above 150 Hz with reasonably good accuracy. It is pointed out, however, that when evaluating the local surface admittance, the mounting conditions of the acoustic lining must be taken into account in the case of absorbing materials, with which the frame cannot be assumed to be motionless. When no additional information about the complex valued surface admittance is available, an absorption coefficient α is not a suitable index to a lining in the low-frequency range. Only when $\mathrm{Re}(\tilde{Y}) < 1$ and $\mathrm{Im}(\tilde{Y}) \approx 0$ holds true can the corresponding absorption coefficient be used to judge the quality of an acoustic lining. This condition is generally satisfied only when the lining is

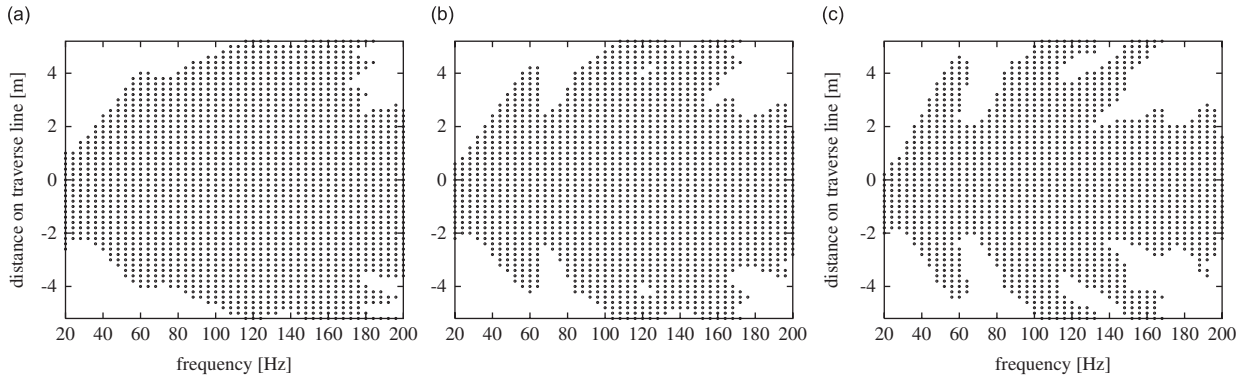

Fig. 8. 1.5 dB region obtained by performing numerical simulations with various local surface admittance values but with almost the same absorption coefficient. Sub-figure (a) $Y_1 = 0.9$ ($\alpha_1 = 0.997$), sub-figure (b) $Y_2 = 1$ ($\alpha_2 = 1.0$) and sub-figure (c) $Y_3 = 1.1$ ($\alpha_3 = 0.997$).

sufficiently absorbent. Especially at low frequencies, the use of the simple local admittance model is not a suitable means of modeling the lining numerically.

3. Localized admittance condition

In the previous section, it was explained why a local surface admittance cannot be used to predict the quality of an anechoic chamber in the low-frequency range. A method is now presented that makes it possible to extend the frequency range in which the 1.5 dB region of an anechoic chamber can be predicted numerically in the chamber planning stage.

The following situation is now considered. Sound propagation within a fluid domain Ω_F is to be treated. This domain Ω_F has a common boundary Γ_Y with a second domain Ω_B occupied by an absorbing material. The influence of the domain Ω_B on the sound field in Ω_F has to be studied, whereas the sound propagation in the domain Ω_B is of less importance. Under these conditions a relation between the vector of the nodal sound pressures $\mathbf{p}^{\Gamma_Y}$ and the nodal normal surface velocities $\mathbf{v}_\mathbf{n}^{\Gamma_Y}$ on the common boundary Γ_Y can be established as follows. The sound propagation in Ω_B is modeled using the equivalent fluid or the Biot model combined with a FEM. By suitably reordering, we can group the unknowns so that $\mathbf{p}^{\Gamma_Y}$ contains all unknown pressures on Γ_Y and $\mathbf{x}_\Omega$ the remaining unknowns. The linear system of equations for the unknown quantities now reads

$$\begin{bmatrix} \mathbf{A}^{\Omega\Omega} & \mathbf{A}^{\Omega\Gamma} \\ \mathbf{A}^{\Omega\Gamma\mathrm{T}} & \mathbf{A}^{\Gamma\Gamma} \end{bmatrix} \begin{bmatrix} \mathbf{x}_\Omega \\ \mathbf{p}^{\Gamma_Y} \end{bmatrix} = \begin{bmatrix} \mathbf{0} \\ \mathbf{M}\mathbf{v}_\mathbf{n}^{\Gamma_Y} \end{bmatrix} \tag{8}$$

Using the Schur complement of $\mathbf{A}^{\Omega\Omega}$ to eliminate $\mathbf{x}_\Omega$ in Eq. (8), one obtains a relation between the surface normal velocity $\mathbf{v}_\mathbf{n}^{\Gamma_Y}$ and the sound pressure $\mathbf{p}^{\Gamma_Y}$ on the surface Γ_Y:

$$\mathbf{p}^{\Gamma_Y} = (\mathbf{A}^{\Gamma\Gamma} - \mathbf{A}^{\Omega\Gamma\mathrm{T}}\mathbf{A}^{\Omega\Omega-1}\mathbf{A}^{\Omega\Gamma})^{-1}\mathbf{M}\mathbf{v}_\mathbf{n}^{\Gamma_Y} \tag{9}$$

Eq. (9) shows that in the general case, the presence of an absorbing material must be accounted for by a non-local boundary condition at the corresponding boundary of the fluid domain Ω_F. The above assumption about the local admittance condition is therefore questionable from the theoretical point of view. Since the discretizations of the domains Ω_B and Ω_F may be different introducing appropriate interpolation matrices to interpolate the nodal values on the different meshes gives the more general equation

$$\mathbf{p}^{\Gamma_Y} = \mathbf{Z}(\omega)\mathbf{v}_\mathbf{n}^{\Gamma_Y} \tag{10}$$

relating the sound pressure to the normal velocity. The dense, frequency dependent matrix $\mathbf{Z}(\omega)$ stands for a non-local impedance condition on the boundary Γ_Y. After a possible regularization, the matrix $\mathbf{Z}$ can be inverted to obtain the relation

$$\mathbf{v}_\mathbf{n}^{\Gamma_Y} = \mathbf{Y}(\omega)\mathbf{p}^{\Gamma_Y} \tag{11}$$

as in Eq. (1). Except for special cases where the discretization of the domain Ω_B requires only a small number of unknowns, such as the case of a small absorbing object embedded in an acoustic fluid, the numerical evaluation of $\mathbf{Y}(\omega)$ in Eq. (11) will be too time-consuming. Hence a suitable method of truncating this matrix must be found. Here the following strategy is suggested. Grouping the sound pressure $\mathbf{p}^{\Gamma_Y}$ into disjunct sets $\mathscr{S}_i$ such that each set $\mathscr{S}_i$ contains a certain number of nodal sound pressures $\mathbf{p}^{\Gamma_Y}_{\mathscr{S}_i}$ on Ω_F yields

$$\mathbf{v}_{\mathbf{n}}^{\Gamma_Y} = \mathbf{Y}\mathbf{p}^{\Gamma_Y} = \sum_i \mathbf{Y}\mathbf{p}^{\Gamma_Y}_{\mathscr{S}_i} = \sum_i \mathbf{Y}^i\mathbf{p}^{\Gamma_Y}_{\mathscr{S}_i} \tag{12}$$

where Y^i denotes the restriction of Y to the set of points $\mathscr{S}_i$. If the domain Ω_B possesses a periodic geometry, then with a suitable choice of the sets $\mathscr{S}_i$, all matrices $\mathbf{Y}^i$ will be identical. However, the matrix $\mathbf{Y}^i$ still couples the set $\mathscr{S}_i$ to all the other points on Γ_Y and is thus still a non-local coupling condition. The localization of this non-local behavior can be achieved by neglecting entries to the vector $\mathbf{v}_{\mathbf{n}}^{\Gamma_Y}$ that correspond to points at a large distance from the set $\mathscr{S}_i$, i.e., keeping only the first n_T rows of $\mathbf{Y}^i$:

$$\mathbf{v}_{\mathbf{n}}^{\Gamma_Y}(\mathbf{p}^{\Gamma_Y}_{\mathscr{S}_i}) \approx \begin{bmatrix} \mathbf{v}_{\mathbf{n}_I}{}^{\Gamma_Y} \\ \mathbf{0} \end{bmatrix} = \begin{bmatrix} \mathbf{Y}^i_{\langle 1:n_T,:\rangle} \\ \mathbf{0} \end{bmatrix} \mathbf{p}^{\Gamma_Y}_{\mathscr{S}_i} = \mathbf{Y}^i_{n_T}\mathbf{p}^{\Gamma_Y}_{\mathscr{S}_i} \tag{13}$$

The rows of $\mathbf{Y}^i$ are assumed to be ordered so that the first n_T rows correspond to points the nearest to the points in the set $\mathscr{S}_i$. The quality of the localization proposed depends greatly on the behavior of the absorbing material. The more absorbent the material is, the smaller the value of n_T can be. The value of n_T therefore determines the accuracy of the approximation as well as the numerical costs. An expression for the truncation error depending on a specific incident sound field can be defined as follows:

$$\varepsilon^{n_T}(p_{\text{inc}}) = \frac{\|(\mathbf{Y}^i - \mathbf{Y}^i_{n_T})p_{\text{inc}}\|}{\|\mathbf{Y}^i p_{\text{inc}}\|} \tag{14}$$

The dependency of the error measure on a given sound field has been introduced to account for the type of application we have in mind. The sound field in an enclosure is not arbitrary. In the low-frequency range of interest here, it can be modeled using a set of monopole sound sources. Therefore, a set of monopole sources placed at a certain distance from the set of points $\mathscr{S}_i$ can be used to generate a sound field that is fairly similar to that of the real application. This sound field can then be used to check the quality of the approximation proposed above.

The quality of the method of localizing the non-local admittance condition presented here was tested using two different materials and the geometry of the acoustic lining at the LMA. Material A is a fibrous polyester material used to manufacture the acoustic linings of anechoic chambers. The acoustic parameters given in Ref. [9] were used for this purpose. The second material is the melamine foam used to make the acoustic lining of the anechoic chamber at the LMA. Both sets of acoustical parameters are given in Table 1. To model the melamine foam, the Biot model [10–14] was used with the additional mechanical parameters $E = 0.16e + 6\,\text{N/m}^2$, $\nu = 0.44$ and $\varrho = 8.35\,\text{kg/m}^3$. Material A was modeled using the equivalent fluid model as suggested in Ref. [9]. Each of the individual elements of the acoustic lining consists of a base $0.3 \times 0.3\,\text{m}^2$ in size and 0.4 m in length and a tapering section 0.7 m in length. Arrays of 7×7 and 9×9 wedges were used in the case of material A. Because of the higher numerical computation costs involved when the Biot model is used instead of the equivalent fluid model for the melamine foam, only arrays consisting of 5×5 and 7×7 wedges were used for these numerical simulations. The incident sound pressure was applied to the central wedge in the

Table 1
Material parameters of the melamine foam and material A

Material	Flow resistivity σ (Ns/m^4)	Porosity Φ	Tortuosity α_∞	Characteristic dimensions	
				Λ (m)	Λ' (m)
Melamine	1.2e4	0.99	1.0	0.8e−4	0.28e−3
Material A	3.0e3	0.98	1.0	0.2e−3	0.3e−3

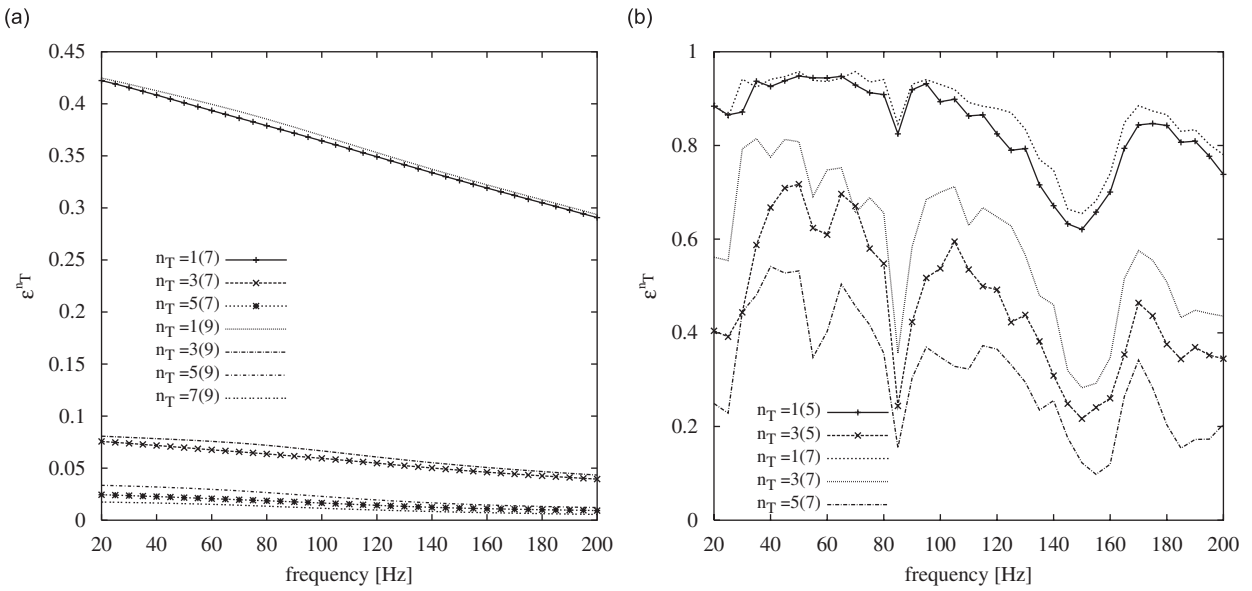

Fig. 9. Truncation error given by Eq. (14) with various values of n_T. The n_T-value gives the size of the truncated array and the number in brackets gives the size of the total array. Sub-figure (a) in the case of material A and sub-figure (b) in that of the melamine foam. Note the difference between the scales of the two sub-figures.

arrays. The error defined in Eq. (14) in the case of the two materials is shown in Fig. 9. With material A, even when the vector $\mathbf{v}_{\mathbf{n}}^{\Gamma_Y}$ is truncated after the central wedge ($n_T = 1$), the error calculated from Eq. (14) is less than 50%. Also, taking the adjacent wedges into account causes the error to decrease to less than 10%. In addition, the error is almost independent of the total size of the array, as the results obtained on arrays of 7×7 and 9×9 wedges were practically identical. The localized admittance therefore provides a very good approximation of the non-local behavior of this material.

The results obtained on the melamine foam were less satisfactory. To obtain a truncation error of less than 50% over the entire frequency range, at least the two adjacent layers of wedges have to be used. The higher level truncation error can be explained by the effects of the sound propagation in the elastic frame of the material. Elastic waves can propagate in the frame without being significantly attenuated, due to the very low level of dissipation occurring in the frame material at low frequencies. However, at frequencies above ≈ 100 Hz, using only the adjacent layer of wedges ($n_T = 3$) results in a truncation error of less than 50%. The domain Ω_B which is used to evaluate the impedance matrix $\mathbf{Z}$ in Eq. (10) was truncated based on value of n_T chosen. This was a necessary compromise between numerical efficiency and accuracy. Taking only the adjacent layer of wedges, i.e. $n_T = 3$, a dense impedance matrix $\mathbf{Z}(\omega) \in \mathbb{C}^{324\times324}$ had to be evaluated and inverted to obtain the admittance matrix $\mathbf{Y}_{n_T} \in \mathbb{C}^{324\times36}$ at each frequency of interest. But taking two adjacent layers of wedges, i.e. $n_T = 5$, an impedance matrix $\mathbf{Z}(\omega) \in \mathbb{C}^{870\times870}$ had to be evaluated and inverted to obtain the admittance matrix. Note that the most costly part of the process of evaluation of the impedance matrix Z is the evaluation of $\mathbf{A}^{\Omega\Omega^{-1}}\mathbf{A}^{\Omega\Gamma}$ in Eq. (9). Here we used a sparse direct solver to solve this system of linear equations. At $n_T = 3$, we had to factorize a system with $N_{\mathrm{FE}} = 137\,000$ and at $n_T = 5$, a system with $N_{\mathrm{FE}} = 205\,000$ unknowns. Using an even larger array of wedges would become prohibitively expensive in terms of the numerical and memory requirements.

The localized admittance condition presented here for modeling the acoustic lining of an anechoic chamber was used to predict the 1.5 dB region of the large anechoic chamber at the LMA. Contrary to what was done in Section 2, the real geometry of the lining will now be taken into account. The lining consists of 3720 melamine wedges as described above. As all the wedges are identical, only a single matrix $Y^i_{n_T}$ is required. However, to account for the anisotropy of the melamine foam, three different matrices $\mathbf{Y}_{n_T}$, representing the three different material orientations were actually used. These matrices were calculated in the 20–200 Hz frequency range with a frequency resolution of 1 Hz. To avoid having to mesh the domain Ω_F (the interior of

the chamber) the BEM was used for the numerical simulations. Implementing the proposed boundary condition in a boundary element code is quite straightforward. The scalar admittance $\mathbf{Y}_i$ in Eq. (6) is generally assembled in a diagonal matrix. This diagonal matrix has to be replaced by a matrix containing the matrix $\mathbf{Y}_{n_T}$ at the corresponding positions.

Each of the wedges was modeled using nine elements, resulting in a mesh size of 0.3 m. The boundary element meshing of a single wedge as well as the meshed geometry used to calculate the impedance matrix $\mathbf{Z} \in \mathbb{C}^{324\times324}$ and the admittance matrix $\mathbf{Y}_{n_T} \in \mathbb{C}^{324\times36}$ used subsequently are shown in Fig. 10. Linear discontinuous basis functions [15] were used together with a multilevel fast multipole [16–18] accelerated collocation method. The linear system of equations with $N = 138\,280$ unknowns was solved using the GMRes [19] solver. Depending on the frequency, 80–120 iterations were necessary to obtain a relative residual of $\varepsilon = 1 \cdot e - 6$, which required a total solution time of less than 1.5 h per frequency on a single processor of the Linux Networx PC-Farm at the Center for Information Services and High Performance Computing of the Technische Universität Dresden, Germany. Numerical results are compared with experimental data in Fig. 11 with the two source positions. Solid dots stand for the numerical results. The bounds of the 1.5 dB region obtained from experimental data are given by a solid line. In the case of both source positions, the numerical and experimental results show good agreement in the 40–200 Hz frequency range. The numerical model accurately predicted the perturbations occurring in the 110–160 Hz frequency range. The above defined

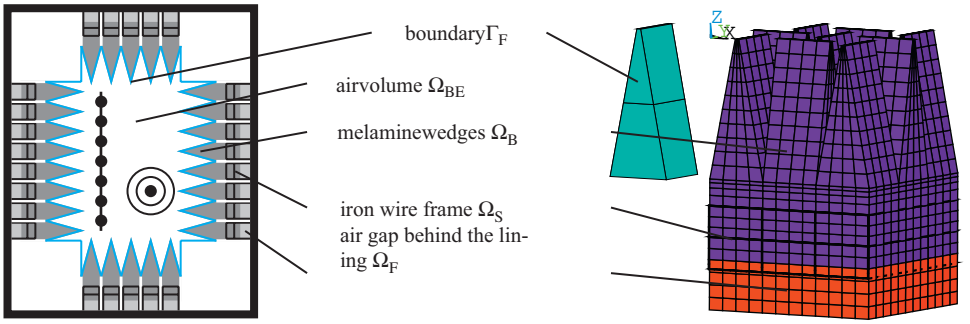

Fig. 10. Diagram of the anechoic chamber, the boundary element meshing of a single wedge and the meshed geometry used to calculate the localized admittance matrix Y_{n_T}.

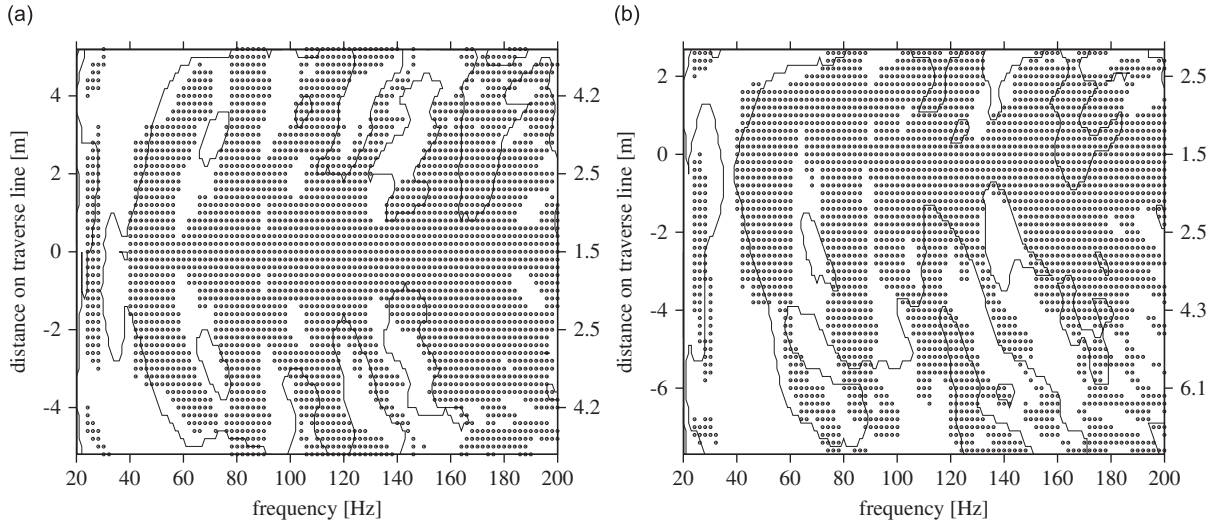

Fig. 11. 1.5 dB region obtained by performing numerical simulations with a localized surface admittance with two different sound source positions. Sub-figure (a) sound source placed in the center of the chamber and sub-figure (b) sound source placed at an eccentric position in the chamber.

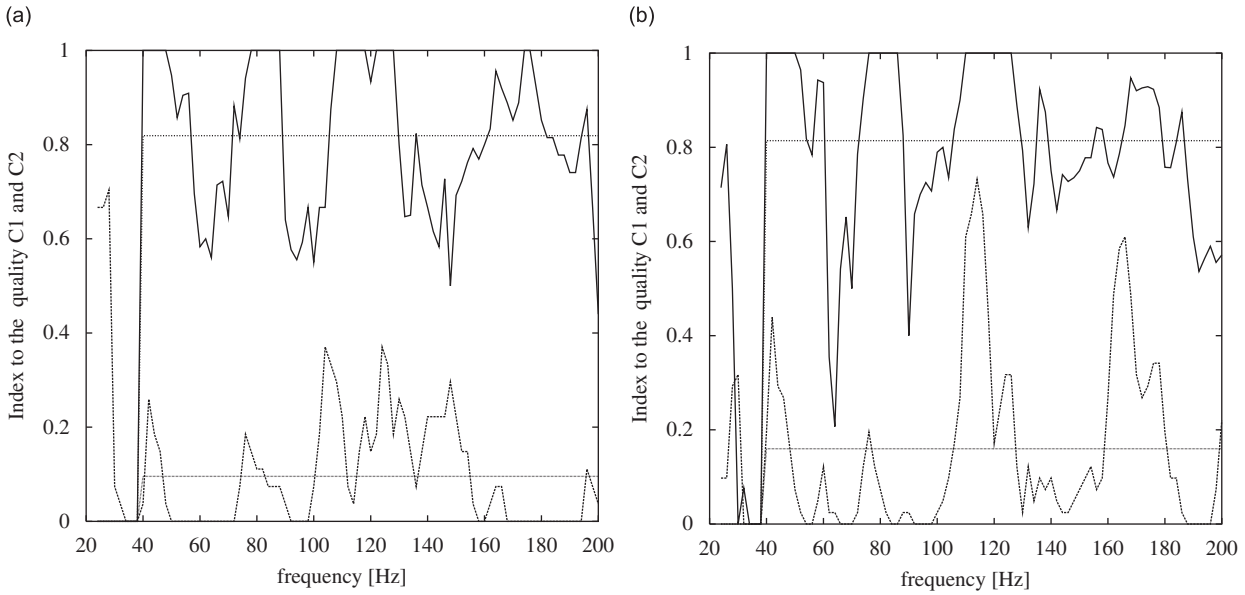

Fig. 12. Index to the quality of the predictions of the 1.5 dB region obtained using the localized surface admittance. Upper curves give indicator C1 and the mean value and lower curves give indicator C2 and the mean value. Sub-figure (a) sound source placed in the center of the chamber and sub-figure (b) sound source placed at an eccentric position in the chamber.

indices to the quality of the numerical predictions indicate that more than 80% of the frequency/position pairs belonging to the 1.5 dB region were correctly predicted by the numerical method using the localized admittance condition proposed here. A value of ≈ 0.1 for the indicator C2 shows that only 10% of the frequency/position pairs were wrongly predicted to belong to the 1.5 dB region of the chamber. The higher rate of errors occurring in the predictions with the source position one in the 160–180 Hz frequency range (see Fig. 12) was due to the asymmetry of the anechoic chamber.

The fact that each frequency required less than $1\frac{1}{2}$ h to be processed with the present numerical model makes this method highly suitable, within limits, for parametric studies on the performances of an anechoic chamber. Parametric studies of this kind can deal not only with the material parameters of the absorbing lining itself, but also with the way in which the lining components are mounted, which can significantly influence the quality of a chamber.

4. Conclusions

Two different approaches to modeling the acoustic lining of an anechoic chamber by performing numerical simulations were tested here. The local admittance model, which is the most commonly used approach, was found to be unsuitable for this purpose in the low-frequency range. At low frequencies, the sound propagation occurring in the absorbing material cannot be neglected as it is when a purely local response of the material is assumed to occur. To account for sound propagation in the material in the case of sound fields that are more general than plane waves, a method of localization of the generally non-local material behavior was developed. In this new model for the acoustic lining, the scalar admittance condition is replaced by an admittance matrix. An error index is also presented here that can be used to estimate the error in this localized boundary condition. The present admittance condition was used to predict the quality of an anechoic chamber numerically in the low-frequency range. These predictions require only previous knowledge of the acoustical and mechanical parameters of the lining. In the case of absorbing materials with an elastic frame, the numerical model presented here is also able to take into account the mounting conditions applied to the future acoustic lining.

Acknowledgments

The author was financed by a grant from the "Deutsche Forschungsgemeinschaft" and by a grant from the French "Agence Nationale de le Recherche" under the Project BLAN06-134753. Numerical simulations were run on a Linux Networx PC-Farmat the Center for Information Services and High Performance Computing at the Technische Universität Dresden, Germany. The author would like to thank C. Kern, who provided the experimental data on the anechoic chamber.

References

[1] F. Sgard, X. Olny, N. Atalla, F. Castel, On the use of perforations to improve the sound absorption of porous materials, *Applied Acoustics* 66 (6) (2005) 625–651.
[2] X. Olny, C. Boutin, Acoustic wave propagation in double porosity media, *The Journal of the Acoustical Society of America* 114 (1) (2003) 73–89.
[3] Y.J. Kang, J.S. Bolton, Finite element models for sound transmission through foam wedges and foam layers having spatially graded properties, *The Journal of the Acoustical Society of America* 98 (5) (1995) 2976.
[4] Y.J. Kang, J.S. Bolton, Sound transmission through elastic porous wedges and foam layers having spatially graded properties, *The Journal of the Acoustical Society of America* 102 (6) (1997) 3319–3332.
[5] V. Easwaran, M.L. Munjal, Finite element analysis of wedges used in anechoic chambers, *Journal of Sound and Vibration* 160 (2) (1993) 333–350.
[6] C.-N. Wang, M.-K. Tang, Boundary element evaluation on the performance of sound absorbing wedges for anechoic chambers, *Engineering Analysis with Boundary Elements* 18 (2) (1996) 103–110.
[7] T. Kar, M. Munjal, Plane wave analysis of acoustic wedges using the boundary-condition-transfer algorithm, *Applied Acoustics* 67 (9) (2006) 901–917.
[8] S. Schneider, C. Kern, Characterization of the large anechoic chamber of the laboratoire de Mécanique et d'Acoustique. *Acustica/Acta Acustica* 94 (1) (2008) 141–147.
[9] X. Olny, Acoustical properties of multiscales absorbing porous materials, *Proceedings of Sapem 2005*, ENTPE Lyon, 2005, pp. 273–286, CD.
[10] M.A. Biot, Theory of propagation of elastic waves in a fluid-saturated porous solid. I. Low-frequency range, *Journal of the Acoustical Society of America* 28 (2) (1956) 168–178.
[11] M.A. Biot, Theory of propagation of elastic waves in a fluid-saturated porous solid. II. Higher frequency range, *Journal of the Acoustical Society of America* 28 (2) (1956) 179–191.
[12] D. Johnson, J. Koplik, R. Dashen, Theory of dynamic permeability and tortuosity in fluid-saturated porous media, *Journal of Fluid Mechanics* 176 (1987) 379–401.
[13] J.-F. Champoux, Y. Allard, Dynamic tortuosity and bulk modulus in air-saturated porous media, *Journal of Applied Physics* 70 (4) (1991) 1975–1979.
[14] N. Atalla, R. Panneton, P. Deberge, A mixed pressure-displacement formulation for poroelastic materials, *Journal of the Acoustical Society of America* 104 (3) (1998) 1444–1542.
[15] S. Marburg, S. Schneider, Influence of element types on numeric error for acoustic boundary elements, *Journal of Computational Acoustics* 11 (3) (2003) 363–386.
[16] V. Rokhlin, Diagonal forms of the translation operators for the Helmholtz equation in three dimensions, *Applied and Computational Harmonic Analysis* 1 (1993) 82–93.
[17] J. Rahola, Diagonal forms of the translation operators in the fast multipole algorithm for scattering problems, *BIT Numerical Mathematics* 36 (2) (1996) 333–358.
[18] E. Darve, The fast multipole method I: error analysis and asymptotic complexity, *SIAM Journal on Numerical Analysis* 38 (1) (2001) 98–128.
[19] Y. Saad, M.H. Schultz, GMRES: a generalized minimal residual algorithm for solving nonsymmetric linear systems, *SIAM Journal on Scientific and Statistical Computing* 7 (3) (1986) 856–869.